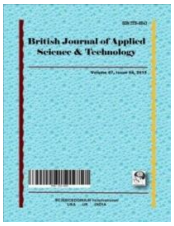

British Journal of Applied Science & Technology
17(1): 1-14, 2016, Article no.BJAST.25787
ISSN: 2231-0843, NLM ID: 101664541

SCIENCEDOMAIN *international*
www.sciencedomain.org

Design of Reactive Power and Voltage Controllers for Converter-interfaced ac Microgrids

Maruf A. Aminu[1*]

[1]*Department of Electrical and Computer Engineering, Curtin University of Technology, Sarawak, Malaysia.*

Author's contribution

The sole author designed, analyzed and interpreted and prepared the manuscript.

Article Information

DOI: 10.9734/BJAST/2016/25787
Editor(s):
(1) Rodolfo Dufo Lopez, Electrical Engineering Department, University of Zaragoza, Spain.
Reviewers:
(1) Boonyang Plangklang, Rajamangala University of Technology Thanyaburi (RMUTT), Thailand.
(2) Bharat Raj Singh, Dr. APJ Abdul Kalam Technical University, Lucknow, India.
Complete Peer review History: http://www.sciencedomain.org/review-history/15689

Original Research Article

Received 20th March 2016
Accepted 5th April 2016
Published 6th August 2016

ABSTRACT

This paper aims at presenting design of two controllers for the study of a microgrid testbed. The response of the microgrid testbed to different short circuits would be investigated under these two control regimes, namely, reactive power and voltage controls. This paper therefore presents design of active power, reactive power and voltage regulators for a converter-interfaced ac microgrid. The design was performed using Simulink Control Design® in the Department of Electrical and Computer Engineering, Curtin University, Sarawak, Malaysia between May 2015 and December 2015. The microgrid consists of two 5.5kW, 575V wind turbines based on doubly-fed induction generators (DFIGs). The systems designed are pitch control system, active power regulator, reactive power regulator, grid ac voltage regulator, dc bus voltage regulator, grid-side converter current regulator and rotor-side converter current regulator. The time-domain step response analysis for each modeled plant indicated stable performance but poor response. Therefore, regulators were realized in closed-loop feedback architecture. Each regulator was designed using small signal frequency response analysis, resulting in stable systems with satisfactory response. The regulators have been combined to implement two mutually exclusive control regimes: the active power-voltage (PV) control and the active-reactive power (PQ) control. Microgrid short circuit studies have been performed while the effect of control is decoupled, a highly simplified method which does not sufficiently mimic real systems. While attempting to study the microgrid short circuit

**Corresponding author: E-mail: maruf.aminu@gmail.com;*

response under different control regimes in a project which is still ongoing, this paper presents an attempt to design two control regimes for the ac microgrid testbed.

Keywords: Microgrid; turbine; generator; controller; converter; DFIG.

NOMENCLATURE

F = prefilter; C = compensator; G = plant; H = sensor; P = proportional; PI = proportional-integral; A_p *= peak amplitude;* $t_{set}(s)$ *= settling time in seconds;* $t_{ris}(s)$ *= rise time in seconds;* $\%\Delta A_p$ *= Per cent improvement in peak amplitude.*

1. INTRODUCTION

The current power system is experiencing increased proliferation of distributed generation (DG) using distributed energy resources in order to increase its reliability and resilience. This trend leads to transformation of the distribution system from passive to active network. Active distribution network based on converter interfacing presents new challenges to the distribution system. These challenges include bidirectional power flow, incapacitating existing protection systems and requirement for advanced control schemes [1-4].

The protection challenge is associated with the limited contribution of the microsources to short circuits as a result of the effect of power electronic converter. When a microgrid is based on converter-interfaced microsource (s), such as the doubly-fed induction generator (DFIG) shown in Fig. 1, its contribution to short circuits (SCs) is limited by the converter capacity if it runs in islanded mode of operation. However, if the microgrid is utility-connected, its contribution to both microgrid and utility faults is limited by both the converter capacity and contribution from the utility's sources. Therefore, the microgrid's contribution to microgrid SCs in islanded mode is not same as its contribution to same fault when in grid-connected mode. This differential contribution to SCs challenges existing protective relays [5-9].

The control challenge is partly because the microgrid lacks the required stored energy (inertia) to quickly recover to a new steady state during and after disturbance such as a short circuit [10-15]. When in grid-connected mode, the microgrid experiences severe oscillation during and after utility disturbance. Also, the control regime determines the contribution of the microgrid to short circuits and its stability during and after disturbances. Implementation of control is, therefore, useful for full-scale deployment of microgrids [16-20].

This paper presents an attempt to implement two basic control strategies for a microgrid based on two 5.5kW converter-interfaced DFIGs. The control strategies are active-reactive power (PQ) control and active power-voltage (PV) control, using a testbed developed in SYMPOWERSystems®. The controllers are designed in order to meet the requirements provided in Table 1.

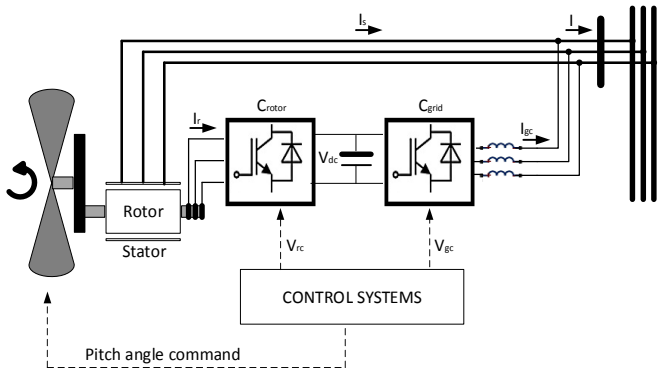

Fig. 1. A simplified DFIG and its connection to the grid

Table 1. Required system specifications

Initial value	0	Final value	1
Rise time	5.00 s	% Rise	90
Settling time	15.00 s	% Settling	1.0
% Overshoot	10.00	% Undershoot	0

2. DESIGN OF CONTROL SYSTEMS

2.1 Active Power Management Systems

2.1.1 Pitch regulator

The open-loop transfer function of the wind turbine is provided in (2.1).

$$G(s)=\frac{K_p}{1+T_p s} \quad (2.1)$$

Where,

$$K_p = 0.20279, T_p = 0.27811.$$

Its step response is shown in Fig. 2.1. It fails to meet the required specifications set in Table 1. A proportional (P) compensator (C) is therefore designed.

The transfer function of the P compensator is provided in (2.2).

$$C=K_p \quad (2.2)$$

Where,

$$K_p = 479.00.$$

Fig. 2.2 shows the closed-loop response of the designed pitch control system. It is a stable loop with infinite gain and phase margins. The system meets the required specifications provided in Table 1.

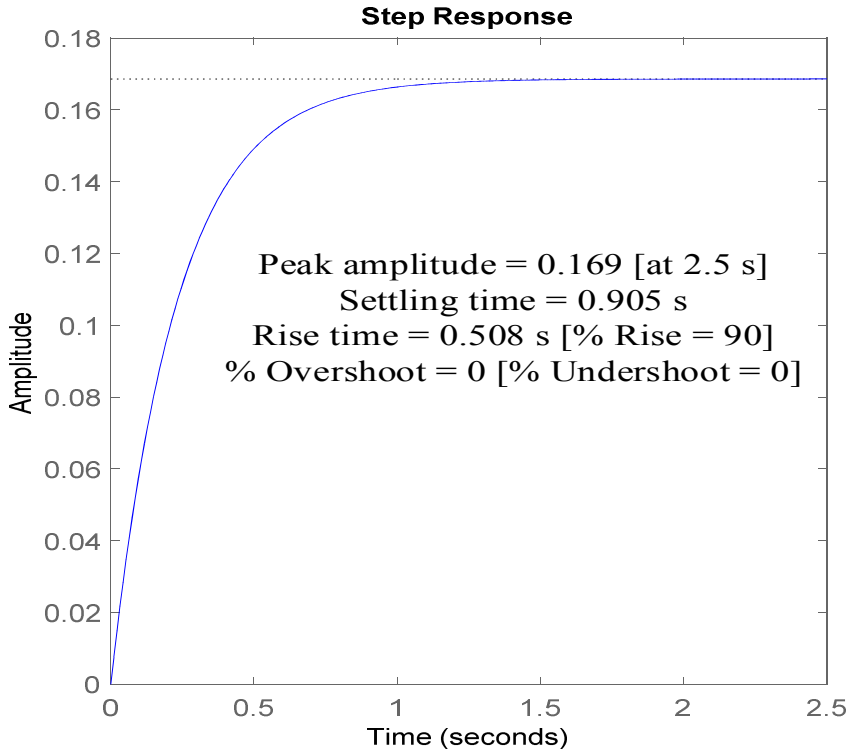

Fig. 2.1. Wind turbine rotor pitch open-loop unit step response

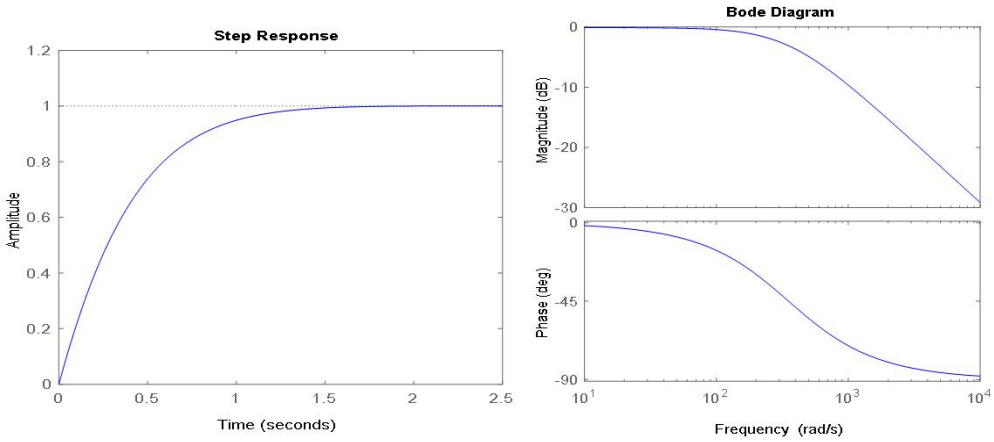

(a) Step response in time domain (b) Bode diagram

Fig. 2.2. Closed-loop response of pitch control system in frequency domain

2.1.2 Active power regulator

The open-loop transfer function of the generator is provided in (2.3).

$$G(s) = \frac{K_p}{(1 + T_{p1}s)(1 + T_{p2}s)} \qquad (2.3)$$

Where,

$$K_p = 863.93, T_{p1} = 8.0351x10^{-5}, T_{p2} = 5x10^{+5}.$$

Its step response is shown in Fig. 2.3. It fails to meet the required specifications set in Table 1. A proportional-integral (PI) compensator is therefore designed as shown in Fig. 2.4.

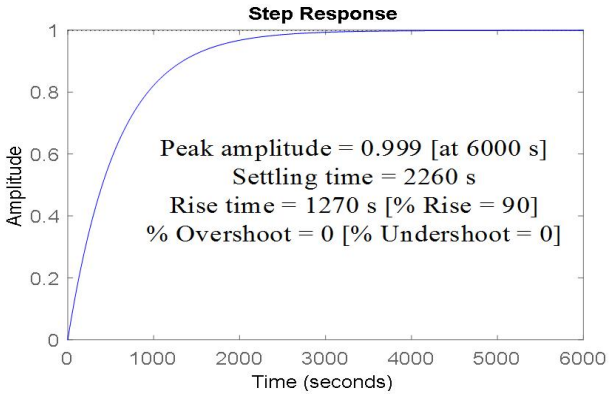

Fig. 2.3. Generator open-loop unit step response

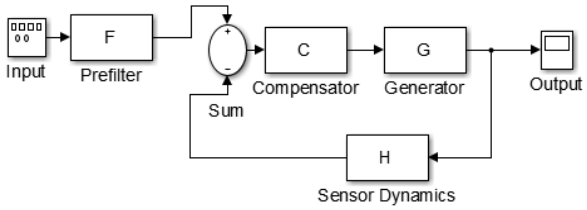

Fig. 2.4. Architecture of active power regulator

The transfer function of the PI compensator is provided in (2.4).

$$C = K_p + \frac{K_i}{s} \tag{2.4}$$

Where,

$$K_p = 578.00, K_i = 0.0026.$$

Fig. 2.5 shows the closed-loop response of the designed PI compensator and generator system. It is a stable loop with infinite gain margin and phase margin of 180° at 0.00223 rads^{-1}. The system meets the required specifications provided in Table 1.

2.2 Reactive Power Management System

The open-loop transfer function of the reactive var source is provided in (2.5).

$$G(s) = \frac{K_p}{1 + T_p s} \tag{2.5}$$

Where,

$$K_p = 5450.10, T_p = 5.724.$$

Its step response is shown in Fig. 2.6.

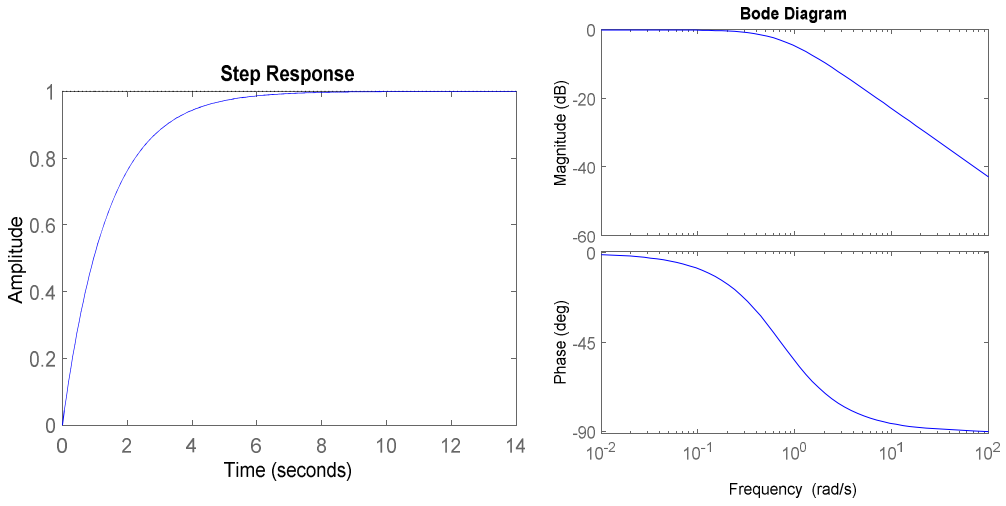

(a) Step response in time domain (b) Bode diagram

Fig. 2.5. Closed-loop response of active power regulator in frequency domain

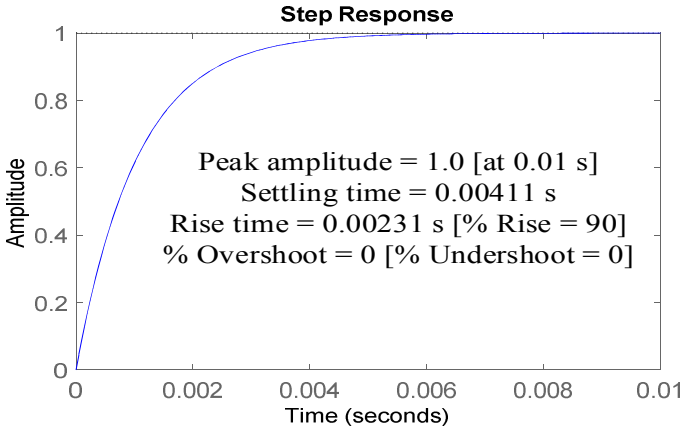

Fig. 2.6. Var source open-loop unit step response

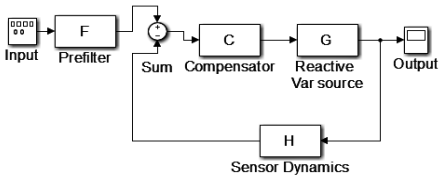

Fig. 2.7. Architecture of reactive power management system

A PI compensator is designed. Its transfer function is provided in (2.6).

$$C = K_p + \frac{K_i}{s} \tag{2.6}$$

Where,

$$K_p = 0.0162, K_i = 0.00214.$$

Fig. 2.8 shows the closed-loop response of the designed reactive power management system. It is a stable loop with infinite gain margin and phase margin of 180° at 0 rads^{-1}. The system meets the required system specifications provided in Table 1.

2.3 Voltage Management Systems

2.3.1 Grid ac voltage regulator

The open-loop transfer function of the voltage source is provided in (2.7).

$$G(s) = \frac{K_p}{1 + T_p s} \tag{2.7}$$

Where,

$$K_p = 0.20, T_p = 0.22375.$$

Its step response is shown in Fig. 2.9.

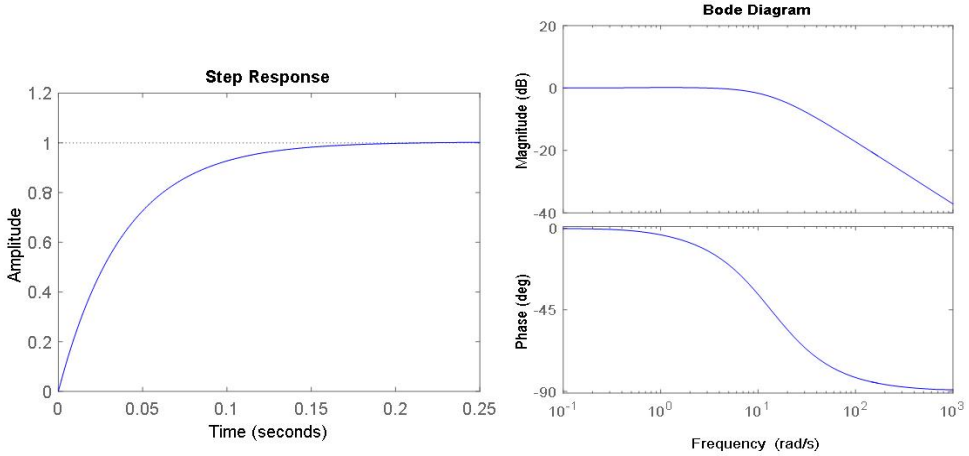

(a) Step response in time domain (b) Bode diagram

Fig. 2.8. Closed-loop response of reactive power management system in frequency domain

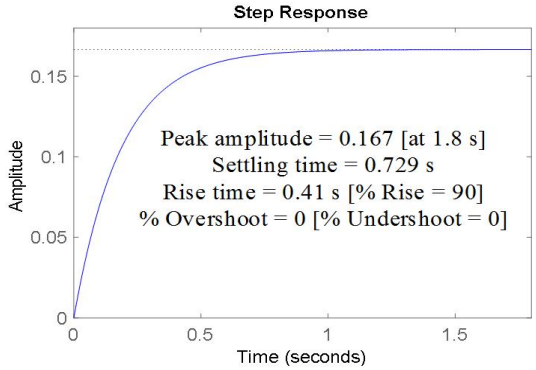

Fig. 2.9. Voltage source open-loop unit step response

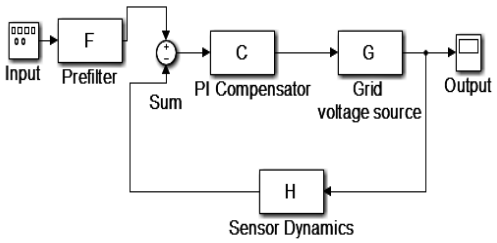

Fig. 2.10. Architecture of grid voltage regulator

A PI compensator is designed. Its transfer function is provided in (2.8).

$$C = K_p + \frac{K_i}{s} \tag{2.8}$$

Where,

$$K_p = 18.30, K_i = 195.00.$$

Fig. 2.11 shows the closed-loop response of the designed grid voltage regulator. It is a stable loop with infinite gain margin and phase margin of 140° at 13.5 rads^{-1}. The system meets the required system specifications provided in Table 1.

2.3.2 DC bus voltage regulator

The open-loop transfer function representing the dc voltage of the rotor-side converter is provided in (2.9). Its open-loop unit step response is provided in Fig. 2.12. A PI compensator whose transfer function is presented in (2.10) is designed such that the converter closed loop meets the requirements in Table 1. Fig. 2.13 shows the closed-loop response of the designed dc bus voltage regulator. It is a stable loop with infinite gain margin and phase margin of 180° at 0 rads^{-1}.

$$G(s) = \frac{K_p}{1 + T_p s} \tag{2.9}$$

Where,

$$K_p = 178.63, T_p = 40000.$$

$$C = K_p + \frac{K_i}{s} \tag{2.10}$$

Where,

$$K_p = 197.00, K_i = 0.00648.$$

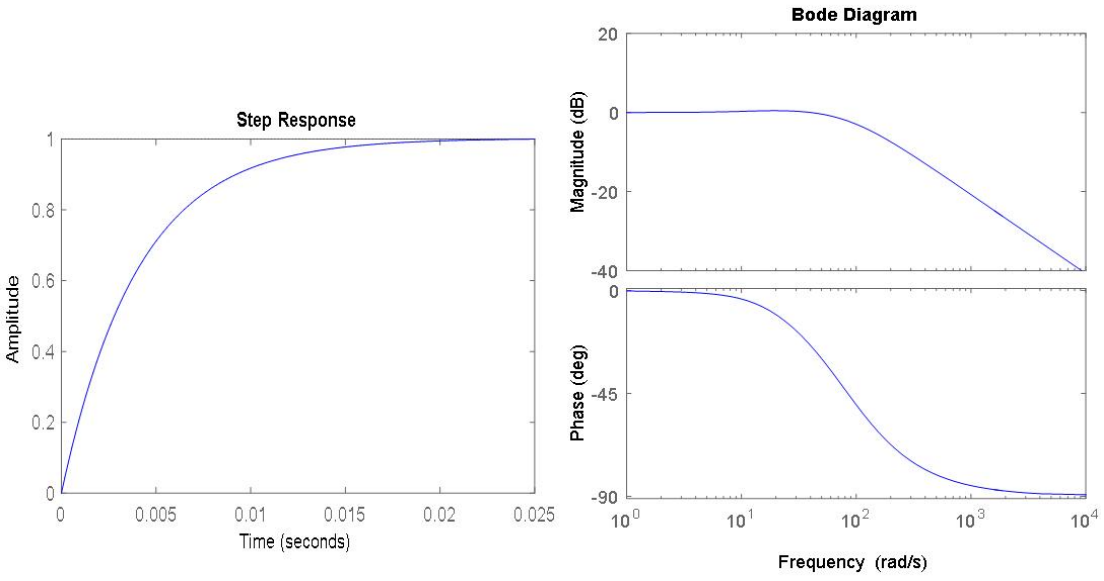

(a) Step response in time domain (b) Bode diagram

Fig. 2.11. Closed-loop response of grid voltage regulator in frequency domain

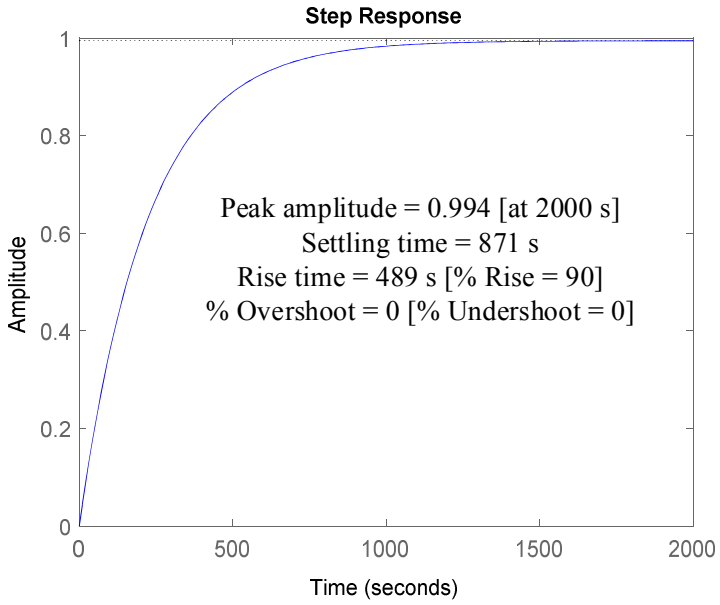

Fig. 2.12. DC bus voltage open-loop unit step response

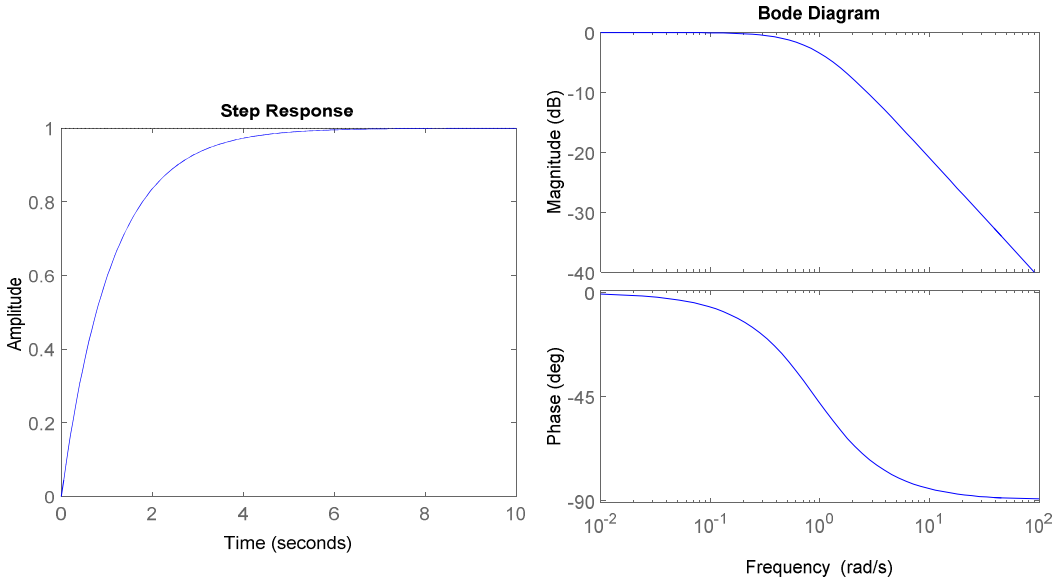

(a) Step response in time domain (b) Bode diagram

Fig. 2.13. Closed-loop response of dc bus voltage regulator in frequency domain

2.4 Converter Current Management Systems

2.4.1 Grid-side converter current regulator

The unit step response of the grid-side converter is shown in Fig. 2.14. Its open-loop transfer function is provided in (2.11).

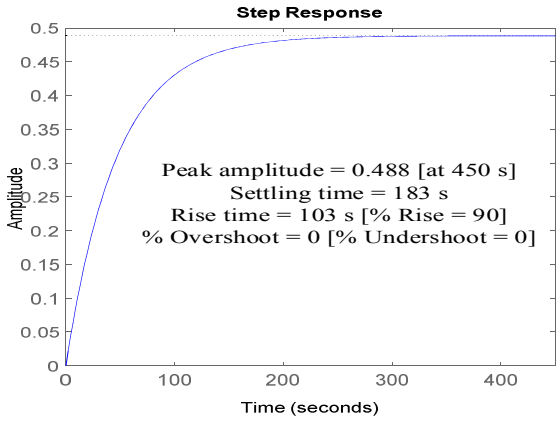

Fig. 2.14. Grid-side converter open-loop unit step response

$$G(s) = \frac{K_p}{1 + T_p s} \tag{2.11}$$

Where,

$$K_p = 0.95516, T_p = 91.698.$$

A PI compensator whose transfer function is presented in (2.12) is designed such that the controller-converter closed loop meets the requirements in Table 1.

$$C = K_p + \frac{K_i}{s} \tag{2.12}$$

Where,

$$K_p = 827.00, K_i = 3.21x10^{-5}.$$

Fig. 2.15 shows the closed-loop response of the designed grid-side converter current regulator. It is a stable loop with infinite gain margin and phase margin of 180° at 0 rads^{-1}. The closed-loop system meets the required system specifications provided in Table 1.

2.4.2 Rotor-side converter current regulator

The unit step response of the rotor-side converter is shown in Fig. 2.16. Its open-loop transfer function is provided in (2.13).

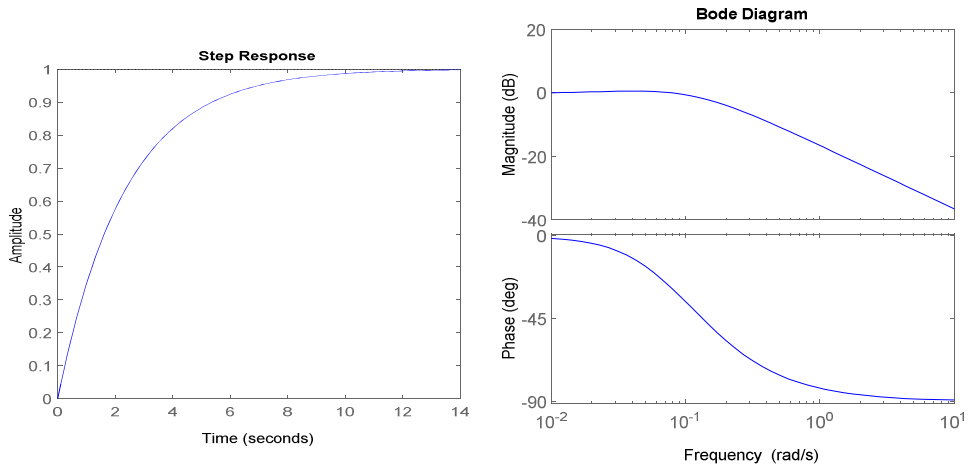

(a) Step response in time domain (b) Bode diagram

Fig. 2.15. Closed-loop response of grid-side current regulator in frequency domain

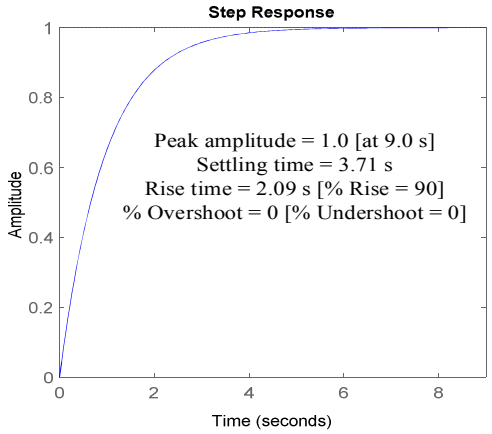

Fig. 2.16. Rotor-side converter open-loop unit step response

$$G(s) = \frac{K_p}{1 + T_p s} \tag{2.13}$$

Where,

$$K_p = 3.8315x10^5, T_p = 3.6368x10^5.$$

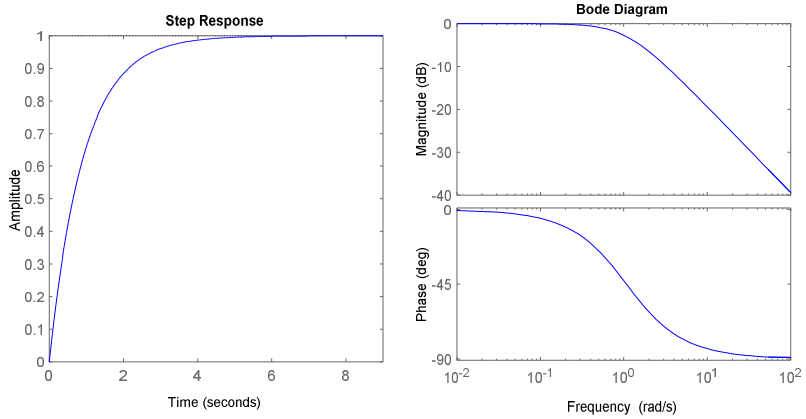

(a) Step response in time domain (b) Bode diagram

Fig. 2.17. Closed-loop response of rotor-side current regulator in frequency domain

A PI compensator whose transfer function is presented in (2.14) is designed such that the controller-converter closed loop meets the requirements in Table 1.

$$C = K_p + \frac{K_i}{s} \tag{2.14}$$

Where,

$$K_p = 0.647, K_i = 4.27x10^{-7}.$$

Fig. 2.17 shows the closed-loop response of the designed rotor-side converter current regulator. It is a stable loop with infinite gain margin and phase margin of 180^o at 0 $rads^{-1}$.

As shown in Table 2, the closed-loop systems meet the required peak value provided in Table 1.

The percent improvement in peak response $\%\Delta A_p$ is given by (2.15).

$$\%\Delta A_p = \frac{\left(A_{pc} - A_{po}\right)}{A_{pc}} x100 \qquad (2.15)$$

Where,

A_{pc} is closed-loop step response and A_{po} is open-loop step response.

Table 2. Summary of system response to unit step signal

Plant	Without regulator			With regulator			
	A_{po} (Peak amplitude)	$t_{set}(s)$ (Settling time)	$t_{ris}(s)$ (Rise time)	A_{pc} (Peak amplitude)	$t_{set}(s)$ (Settling time)	$t_{ris}(s)$ (Rise time)	$\%\Delta A_p$ (Improvement in A_p)
Wind turbine	0.169 at 2.5s	0.905	0.508	1.0 at 2.5s	1.51	0.748	83.10
Active power source (generator)	0.999 at 6000s	2260	1270.00	1.0 at 14s	9.55	2.45	0.10
Capacitive reactive power source	1.0 at 0.01s	0.00411	0.00231	1.0 at 0.25s	0.233	0.0761	0.00
Grid ac voltage source (generator)	0.167 at 1.8s	0.729	0.41	1.0 at 0.025s	0.022	0.00821	83.33
DC bus voltage source (C_{rotor})	0.994 at 2000s	871.00	489.00	1.0 at 2000s	11.12	3.00	0.60
Grid ac current source (C_{grid})	0.488 at 450s	183.00	103.00s	1.0 at 450s	9.45	2.67	51.20
Rotor-side dc current source (C_{rotor})	1.0 at 9.0s	3.71	2.09	1.0 at 9.0s	2.55	1.10	0.00

2.5 Implementation of Control Strategies

The converter is used for power control. The composite ac-ac converter consists of two converters, namely, ac-dc (rotor side) and dc-ac (grid side) converters.

2.5.1 Power and pitch control systems

The pitch angle is maintained constant at zero degree until the speed reaches point D of the tracking characteristic. After point D, the pitch angle is proportional to the speed deviation from point D speed. The control system is shown in Fig. 2.18.

The power is controlled so as to follow a pre-defined characteristic, called power-speed characteristic, as shown in Fig. 2.19.

2.5.2 Rotor-side converter control system

The rotor-side converter is used to control the wind turbine output power and the voltage (or reactive power) measured at the grid terminals, as shown in Fig. 2.20.

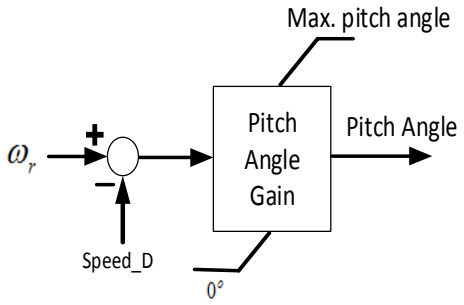

Fig. 2.18. Pitch angle control system

2.5.3 Grid-side converter control system

Fig. 2.21 depicts the grid-side converter. The converter is used to inject or absorb reactive power and to regulate the voltage of the dc bus capacitor.

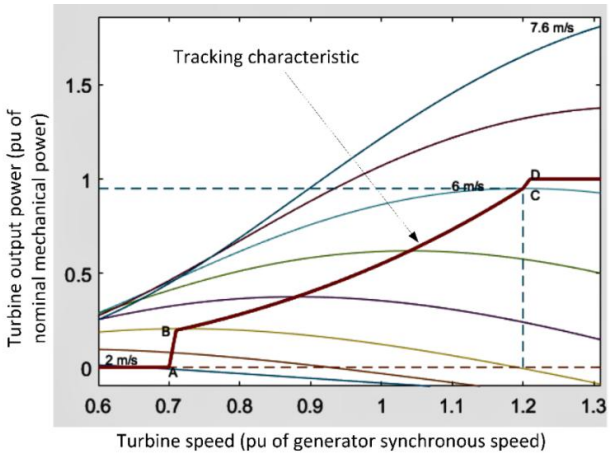

Fig. 2.19. Turbine power characteristics (pitch angle $\beta = 0$)

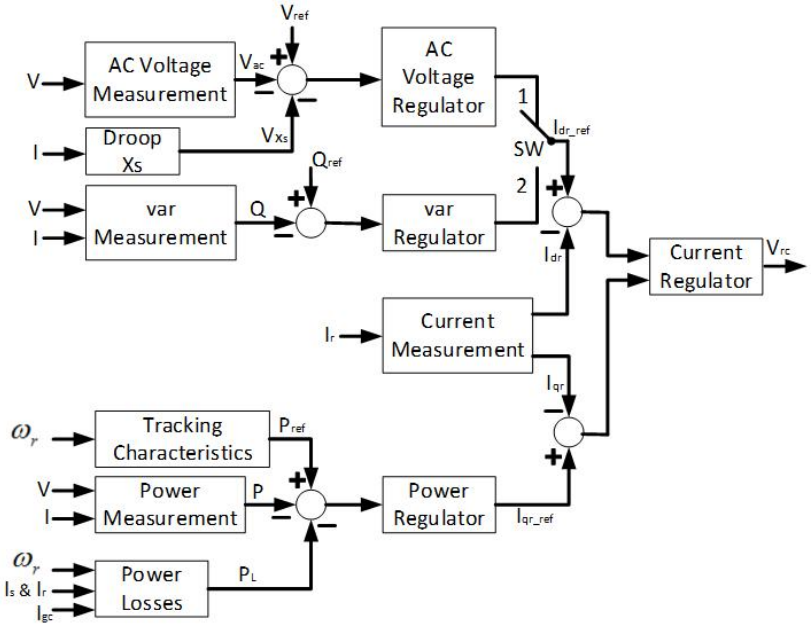

Fig. 2.20. Rotor-side converter voltage and reactive power control systems

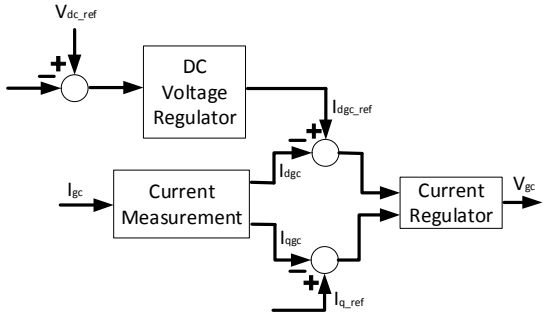

Fig. 2.21. Grid-side converter dc bus voltage and reactive power control systems

3. RESULTS AND DISCUSSION

The generator open-loop unit step response shown in Fig. 2.3 is indicative of a stable system with poor response. A PI feedback regulator is therefore designed to improve its response while retaining its stability, as shown in Fig. 2.4. Fig. 2.5 depicts the closed-loop step response of the active power regulator in time and frequency domains. Each of the regulators in this report has been designed to improve the response of its plant while ensuring that the plant remains stable, as shown in Table 2.

The wind energy captured by the wind turbine is converted into electrical power by the induction generator. The generated power is wheeled to the grid via the stator and rotor windings. In order to control the wind turbine mechanical power, the designed pitch angle control system generates the *pitch angle command* (Fig. 2.18) to control the turbine blade. The power is controlled to follow a predefined power-speed characteristic, called tracking characteristic. The power-speed characteristic used is depicted in Fig. 2.19. It shows the tracking characteristic (ABCD) superimposed on the mechanical power characteristics of the turbine at different wind speeds. For the power control loop (Fig. 2.20), the actual speed of the turbine ω_r is measured and the corresponding mechanical power of the tracking characteristic is computed and used as reference power. The error obtained from the reference power (P_{ref}), measured power (P) and power losses (P_L) is used to generate the rotor-side converter voltage command. The governing control strategy is exclusively PV or PQ control and it is determined by the position of switch SW shown in the figure. When SW is in position 1, PV control is selected. When in position 2, PQ control prevails.

The AC/DC/AC converter has been realized in two stages: the rotor-side converter (C_{rotor}) and the grid-side converter (C_{grid}). C_{rotor} and C_{grid} are Voltage-Sourced Converters which use forced-commutated power electronic devices (IGBTs) for voltage synthesis. A capacitor is linked to the dc bus to serve as dc voltage source. C_{grid} is integrated to the grid via a coupling inductor. The capacitance of the capacitor and the inductance of the inductor are realized from the design of converter voltage and current regulators, respectively. In order to control the dc bus voltage and the reactive power (or the voltage) at the grid terminals, the rotor-side converter control system generates the *voltage command* V_{rc} (Fig. 2.20) to control C_{rotor}, while the grid-side converter control system generates the *voltage command* V_{gc} (Fig. 2.21) to control C_{grid}.

4. CONCLUSION

In this work, requisite controllers for the plants in an ac microgrid have been designed using closed-loop feedback topology. The controllers consist of active power management systems, reactive power management system, voltage management systems and converter current management systems. The regulators have been combined to implement two mutually exclusive control regimes: the active power-voltage (PV) control and the active-reactive power (PQ) control. The small-signal responses of the systems have also been investigated and articulated. The percent improvement in the peak step responses of the plants as a result of the designed regulators has also been presented. Consequently, design of reactive power and voltage controllers for converter-interfaced ac microgrid has been realized.

COMPETING INTERESTS

Author has declared that no competing interests exist.

REFERENCES

1. Oudalov A, et al. Microgrid Protection, in Microgrids. John Wiley and Sons Ltd. 2013;117-164.
2. Chowdhury S, Chowdhury SP, Crossley P, Distributed Energy Resources, in Microgrids and Active Distribution Networks. Institution of Engineering and Technology; 2009.
3. Schwaegerl C, Tao L. Quantification of Technical, Economic, Environmental and Social Benefits of Microgrid Operation - Microgrids. John Wiley and Sons Ltd. 2013;275-313.
4. Jahangir Hossain AM. Renewable Energy Integration - Challenges and Solutions, Singapore; 2014.
5. Edward Coster JM, Wil Kling. Effect of DG on distribution grid protection, in Distributed Generation. Netherlands. 2010;28.
6. Nikkhajoei H, Lasseter RH. Microgrid Protection. in 2007 IEEE Power Engineering Society General Meeting; 2007.

7. Ustun TS, Ozansoy C, Zayegh A. A microgrid protection system with central protection unit and extensive communication. in 2011 10th International Conference on Environment and Electrical Engineering (EEEIC); 2011.
8. Hatziargyriou, NAAH, Iravani R, Marnay C. Microgrids. IEEE Power and Energy Magazine. 2007;5(4):78-94.
9. Dewadasa M. Protection of Distributed Generation Interfaced Networks. Queenslan University of Technology: Queensland. 2010;179.
10. Pecas Lopes JA. Advanced MicroGrids as a component for active management of distribution networks. in 2009 International Conference on Power Engineering, Energy and Electrical Drives, POWERENG *'09;* 2009.
11. Piagi P, Lasseter RH. Autonomous control of microgrids. in 2006 IEEE Power Engineering Society General Meeting; 2006.
12. Zamora R, Srivastava AK. Controls for microgrids with storage: Review, challenges, and research needs. Renewable and Sustainable Energy Reviews. 2010;14(7):2009-2018.
13. Peças Lopes JA, Moreira CL, Madureira AG. Defining control strategies for MicroGrids islanded operation. IEEE Transactions on Power Systems. 2006; 21(2):916-924.
14. Planas E, et al. AC and DC technology in microgrids: A review. Renewable and Sustainable Energy Reviews. 2015;43: 726-749.
15. Planas E, et al. General aspects, hierarchical controls and droop methods in microgrids: A review. Renewable and Sustainable Energy Reviews. 2013;17: 147-159.
16. Lopes JAP, et al. Integrating distributed generation into electric power systems: A review of drivers, challenges and opportunities. Electric Power Systems Research. 2007;77(9):1189-1203.
17. Degner T, et al. Intelligent Local controllers, in microgrids. John Wiley and Sons Ltd. 2013;81-116.
18. Hatziargyriou N, et al. Microgrids. IEEE Power and Energy Magazine, 2007;5(4): 78-94.
19. Lasseter RH. Micro Grids. in 2002 IEEE Power Engineering Society Winter Meeting; 2002.
20. Schwaegerl C, Tao L. The Microgrids Concept. John Wiley and Sons Ltd. 2013; 1-24.

Peer-review history:
The peer review history for this paper can be accessed here:
http://sciencedomain.org/review-history/15689